crystals

MDPI

Article

Homogeneous Organic Crystal Nucleation Rates in Solution from the Perspective of Chemical Reaction Kinetics

Sven L. M. Schroeder [1,2,3]

[1] School of Chemical and Process Engineering, University of Leeds, Leeds LS2 9JT, UK; s.l.m.schroeder@leeds.ac.uk
[2] Diamond Light Source, Harwell Science & Innovation Campus, Didcot OX11 0DE, UK
[3] Future Continuous Manufacturing and Advanced Crystallisation (CMAC) Hub, Research Complex at Harwell (RCaH), Harwell Science & Innovation Campus, Didcot OX11 0FA, UK

Abstract: It is demonstrated for 11 different combinations of organic solutes and solvents that the supersaturation dependence of homogeneous organic crystal nucleation rates from solution can be predicted from the solubility, bar a single empirical rate constant, when it is assumed that nucleation takes place in reversible aggregates of solvated solutes formed in supersaturated solutions. Reversible solute aggregation represents natural solute density fluctuations that take place in any solute/solvent system. For thermodynamically ideal solutions, the steady state size distribution, and thus the population of reversible aggregates in supersaturated solution, can be predicted quantitatively from the overall solute concentration by a simple mathematical expression. Supersaturation creates an excess of reversible aggregates with sizes exceeding that of the largest aggregate in saturated solution. It is shown that the number of these excess aggregates is proportional to experimental homogeneous nucleation rates, suggesting a rate equation for homogeneous nucleation that has only one empirical parameter, namely, a rate constant specific to the solute/solvent combination. This rate constant can be determined from standard nucleation rate data. The system-specificity of homogeneous nucleation rates thus appears to be encoded solely in a rate constant for the transformation of the large excess aggregates into crystal nuclei. The driving force for triggering nucleation events in these aggregates is likely the extremely high local supersaturation, which provides the conditions for spatiotemporally aligned bond-breaking (e.g., de-solvation) and bond-forming (e.g., solute–solute bonding) events that create stable crystal nuclei. The possible influence of heterogeneous nucleation by solid impurities is considered.

Keywords: crystallization; homogeneous nucleation; solvation; absolute rate theory; transition state theory; desolvation; phase separations; solute speciation; solute–solvent interactions

Citation: Schroeder, S.L.M. Homogeneous Organic Crystal Nucleation Rates in Solution from the Perspective of Chemical Reaction Kinetics. *Crystals* **2024**, *14*, 349. https://doi.org/10.3390/cryst14040349

Academic Editor: Weiwei Tang

Received: 16 October 2023
Revised: 3 April 2024
Accepted: 4 April 2024
Published: 6 April 2024

1. Introduction

Across the chemical sciences, rate processes involving interactions between solutes in solutions are modelled in the framework of reaction kinetics and absolute rate theory (often also referred to as transition state theory) that was developed in the early 20th century [1–5]. In contrast, the mainstream of research on crystal nucleation and growth has adopted classical nucleation theory (CNT) for modelling of homogeneous crystal nucleation rates from solutions [6–13]. CNT was originally developed for predicting the rates of phase transitions in single component systems, such as the formation of liquid water droplets from supersaturated water vapor or crystallization from melts [8,14–17]. It has played a crucial role in developing a quantitative understanding of nucleation rates in these systems [17,18]. CNT focuses on the thermodynamic stability of the final state of the nucleation process, specifically, the stability of nuclei formed by collisions of molecules in a supersaturated, thermodynamically metastable phase. It treats nucleation as an activated process in which the formation of stable nuclei of a new phase is principally hindered by an interfacial free energy penalty. Nuclei become thermodynamically stable only after

growing beyond a critical size, at which their cohesive energy exceeds the interfacial energy term. Supersaturation facilitates nucleation because it increases the chemical potential of the molecules in the metastable phase and thereby reduces the activation barrier to the formation of thermodynamically stable nuclei.

Since the early days of applying CNT to analyzing homogeneous nucleation rates in condensed systems [19], these model principles have been retained to describe the nucleation of crystals from solutions, i.e., the separation of solute molecules from a supersaturated solution [6,10,20]. The crystal nucleation process in solution is thereby, in effect, treated as a condensation of a crystalline phase through diffusively driven collisions between solute monomers in solution. As in CNT for single component systems, the balance between the interfacial and cohesive energy of the nuclei determines the activation barrier to the formation of supercritical stable crystal nuclei, while solute supersaturation reduces the activation barrier by increasing the chemical potential [6,7,10,13,21].

CNT does not explicitly include a molecular-level view of how elementary activation barriers associated with transitioning solvated solute molecules into ordered nuclei of fully or partially de-solvated solutes are overcome [7], which creates a substantial, indeed principal, barrier to relating modern theoretical analyses, e.g., by molecular dynamics, to measured nucleation rates [22]. In this paper, the rates of homogeneous nucleation from solution will therefore be explored through the lens of chemical kinetics and absolute rate theory [1–5], which intrinsically create a quantitative mechanistic link between the macroscopically observable rates of product formation and both the frequency and nature of elementary molecular interactions. The key assumption of absolute rate theory is that the overall rate is determined by an equilibrium between reactants (here: organic solute molecules) and the transition state, which is the assembly of molecules associated with the lowest energy barrier for crossing from the initial (here: solvated solutes in a supersaturated solution) to the final state (here: supercritical nuclei surrounded by a saturated solution) of the rate process [1–5]. More formally put, the transition state represents the molecular configuration at a saddle point on the potential energy surface for all possible molecular configurations of the system. The local ultrafast molecular dynamics in the transition state, i.e., bond-breaking and bond-forming events, then determine the overall rate [23,24]. The nature of the relevant bond-breaking and forming events may be influenced by any inter- and intramolecular interactions such as London interactions, rotations, vibrations, electrostatics, and electronic transitions.

In this paper, a mathematically simple yet quantitative homogeneous nucleation rate equation with only one a priori unknown parameter, namely, a system-specific nucleation rate constant, will be derived. The rate constant can then be interpreted in terms of the classical chemical rate theory framework, including its Arrhenius dependence on temperature with an activation energy and a pre-exponential factor. Knowledge of the rate constant at a given temperature permits the prediction of homogeneous nucleation rates from the solubility at that temperature. Central to deriving the alternative homogeneous nucleation rate equation are diffusively driven microscopic solute density fluctuations in solutions, which are akin to other manifestations of microscopic fluctuations, most famously, Brownian motion [25,26]. Solutions contain a diffusively driven steady-state population of short-lived microscopic regions with a high local density of solvated solute molecules. The potential importance of these regions, which are often referred to as reversible aggregates, for nucleation phenomena has been recognized for some time [27–34], but their connection to chemical rate theory has not been realized. These regions form and dissolve reversibly on time scales comparable to that of diffusive solute–solute collisions, i.e., on the order of nanoseconds. In these aggregates, the integrity of the solvation shells around the solute molecules is largely unperturbed, so solute–solute collisions create merely spatial proximity of the solvated solute molecules without significant attractive interactions. The aggregates are therefore truly reversible and should therefore not be confused with the formation of metastable phases, such as pre-nucleation clusters and observable pre-nucleation phases that are widely discussed in the contemporary research on non-classical

nucleation pathways [7,12,35–46]. Diffusively driven reversible aggregates of solvated solutes are also distinct from weakly coagulated phases formed by colloidal interactions that are, confusingly, often called reversible aggregates as well [28,29,47].

In the following sections of this paper, it will be shown how, for an ideal solution, the steady-state size distribution of reversible aggregates can be predicted quantitatively from the overall solute concentration. Supersaturation is associated with the formation of aggregate sizes beyond that of the largest aggregate in a saturated solution. The supersaturation dependence of homogeneous crystal nucleation rates in solution will be shown to be proportional to the number of these excess large aggregates. This observation then informs the central mechanistic hypothesis of this paper, namely, that the high local solute density in these large reversible aggregates allows the specific spatiotemporal alignment of solute molecules in the transition state for homogeneous nucleation from solution, which is characterized by the system-specific nucleation rate constant. The high local density of solvated solute molecules is thus assumed to allow spatiotemporally coordinated ordering, solute–solute bond formation, and solute–solvent bond breaking that creates the stable nucleus. This represents a hypothetical alternative view of homogeneous nucleation from solution that sets the scene for testing by modern experimental studies, e.g., probing the ultrafast molecular dynamics that determine the structure of a stable nucleus, as well as modelling, e.g., molecular dynamics simulations with statistical mechanics elucidating the nature of the transition state.

2. Model

2.1. Reversible Aggregation of Solvated Solutes in Solution

The steady-state size distribution of reversible aggregates in a solution can be calculated for any given solute concentration using elementary kinetic rate theory [1,2], as follows. Generally, a solute dimerization equilibrium in solution,

$$2\mathrm{M} \rightleftharpoons \mathrm{M}_2, \tag{1}$$

is associated with an equilibrium constant, K_2, that determines the equilibrium activities a_2 and a_1 of dimers and monomers, respectively, according to

$$K_2 = \frac{a_2}{a_1^2}. \tag{2}$$

The activity a_3 of trimers formed by monomer attachment to a dimer,

$$\mathrm{M}_2 + \mathrm{M} \rightleftharpoons \mathrm{M}_3, \tag{3}$$

is given by an equilibrium constant, K_3, which, with Equation (2), can also be expressed in terms of K_2 and the monomer activity a_1,

$$K_3 = \frac{a_3}{a_2 a_1} = \frac{a_3}{K_2 a_1^3}. \tag{4}$$

Attachment of further monomers to form higher aggregates with n monomers leads to a general equilibrium expression, for $n > 2$, of

$$K_\mathrm{n} = \frac{a_\mathrm{n}}{a_{\mathrm{n}-1} a_1} = \frac{a_\mathrm{n}}{(K_2 \times K_3 \times \ldots \times K_{\mathrm{n}-1}) a_1^n}. \tag{5}$$

When monomer attachment is reversible, the rate constant k_1 for attachment and the dissociation rate constant k_{-1} for the release of a monomer are equal, resulting in equilibrium constants $K_n \approx K = k_1/k_{-1} = 1$. Equation (5) thus simplifies for reversible aggregation to

$$K^{n-1} = \frac{a_\mathrm{n}}{a_1^n}. \tag{6}$$

With $K = 1$, one obtains the equality

$$a_{\mathrm{n}} = a_1^n. \tag{7}$$

In an ideal solution of solvated solutes, the size distribution of reversible aggregates is determined by the overall activity, a_0, of the solution through the mass balance relating a_0 and the activities, a_n, of the reversible aggregates:

$$a_0 = \sum_{n=1}^{\infty} n a_{\mathrm{n}}. \tag{8}$$

With Equation (7), it follows that

$$a_0 = \sum_{n=1}^{\infty} n a_1^n \tag{9}$$

As shown in the Supplementary Information SI1, evaluating the power series on the right of this equation leads to a simple expression for the equilibrium concentrations $[\mathrm{M_n}]$ (in units of mol dm^{-3}) of reversible aggregates of size n in an ideal solution with an overall concentration $[\mathrm{M}]_0$ (again, in mol dm^{-3}):

$$[\mathrm{M_n}] = \left(\frac{\sqrt{4[\mathrm{M}]_0 + 1} - 1}{\sqrt{4[\mathrm{M}]_0 + 1} + 1} \right)^n. \tag{10}$$

The size distribution of the reversible aggregates is determined only by the overall concentration $[\mathrm{M}]_0$; hence, Equation (10) is universally applicable to any solution containing a single solute species. Solutions of phases with more than one component, e.g., co-crystals or ionic crystals forming cations and anions in solution, will require a modified approach.

For a given temperature and pressure, the solubility concentration defines a system-specific equilibrium size distribution of reversible aggregates, $[\mathrm{M_n}]^*$, according to Equation (10), which extends to a maximum aggregate size containing n^* solvated solute molecules. Solubility thus provides, at a given temperature and pressure, a reference state for quantifying the effect of supersaturation on the reversible aggregate concentrations, $[\mathrm{M_n}]$. The largest aggregate size present in a saturated solution, n^*, can be predicted from Equation (10) by using the condition that N_{n^*}, the number of aggregates with size n^*, in a solution with the volume V must be at least 1,

$$N_{\mathrm{n}^*} = [\mathrm{M_{n^*}}] N_A V = 1, \tag{11}$$

where N_A is Avogadro's number. Replacing $[\mathrm{M_{n^*}}]$ according to Equation (10) gives the maximum aggregate size in saturated solution as (Supplementary Information, SI2)

$$n^* = -\frac{\ln(N_A V)}{\ln\left(\frac{\sqrt{4[\mathrm{M}]_0 + 1} - 1}{\sqrt{4[\mathrm{M}]_0 + 1} + 1} \right)}. \tag{12}$$

2.2. Nucleation from Reversible Aggregates with First Order Kinetics

The number, N, of reversible aggregates contributing to the homogeneous nucleation rate from a supersaturated solution volume, V, is given by

$$N = N_A V \sum_{n=1}^{\infty} \varphi(n) \left([\mathrm{M}_n] - [\mathrm{M_n}]^* \right) \tag{13}$$

where $\varphi(n)$ is an n-dependent weighting function that accounts for the fact that larger reversible aggregates are probably more likely to form stable crystal nuclei. The variations of φ with n are likely to depend on the aggregate lifetime and availability of a sufficient

number of solute molecules for building the transition state for a stable nucleus. $\varphi(n)$ is expected to increase with n, but the exact relationship between aggregate size, n, and nucleation rates, and hence $\varphi(n)$, is currently not known. As a pragmatic choice, which will be justified in Section 3.1 by analysis with Equation (10), $\varphi(n)$ will be modeled as a step function with $\varphi(n < n^*) = 0$ and $\varphi(n \geq n^*) = 1$. Thereby, in effect, only aggregates with a size equal or larger than n*, i.e., the largest aggregate present in the saturated solution, are assumed to contribute to the nucleation rate. Of course, aggregates slightly smaller than n* may also contribute to the rate, while aggregates larger than n* will probably contribute more as their size increases. Through the choice of a cutoff at n*, these effects likely compensate each other, at least in part.

Applying this step function for $\varphi(n)$ allows the calculation of the excess N* of reversible aggregates contributing to the homogenous nucleation rate in a solution of volume V, through

$$N^* = N_A V \sum_{n=n^*}^{\infty} \left([\mathrm{M}_n] - [\mathrm{M}_\mathrm{n}]^* \right) \tag{14}$$

If the reversible aggregates included in N* transform to a stable crystal by first order kinetics with a rate constant k* (in units of s^{-1}), then the nucleation rate, J^* (in units of $m^{-3}\ s^{-1}$), is simply k* multiplied by the number density N^*/V (in units of m^{-3}), according to

$$J^* = k^* \frac{N^*}{V} = k^*\ N_A \sum_{n=n^*}^{\infty} \left([\mathrm{M}_n] - [\mathrm{M}_\mathrm{n}]^* \right). \tag{15}$$

This expression represents a new homogeneous nucleation rate equation, for nucleation from the excess of large reversible aggregates formed in supersaturated solutions. The concentrations $[\mathrm{M}_n]$ and $[\mathrm{M}_\mathrm{n}]^*$ of large excess aggregates are readily calculated from the solubility via Equation (10). Only the first order rate constant k^* is a priori unknown and must be determined empirically by finding best agreement of J^* with experimental nucleation rates, J. The latter are commonly reported in the same units as J^*, namely, the average number N of nuclei formed per solution volume V and time t [21].

2.3. Heterogeneous Nucleation

It is well established that liquid solutions almost inevitably contain microscopic solid impurities whose surfaces promote heterogeneous nucleation [48–50] and that solid additives can influence the outcome of crystallization processes [13,51,52]. Nucleation centers at the solid surface, such as defects or other sites with high local energy, can create nucleation pathways with lower activation barriers than in homogeneous nucleation. Heterogeneous nucleation rates can be higher because the incipient nucleus at a surface is stabilized by the surrounding interfacial and sub-surface atoms of the solid particle. Their effect is included in CNT through a modified interfacial energy term [7,13,49,53]. Indeed, an analysis of the influence of particulate impurities using CNT suggests that real-world crystal nucleation processes in solution are always likely to be heterogeneous due to the presence of microscopic solid impurities [49]. Occasionally, this hypothesis has been checked in nucleation rate studies. An example relevant for the present paper is the case of isonicotinamide nucleation from ethanol, where removal of particles larger than 0.45 μm by solution filtering reduced the nucleation rate somewhat, by approximately a factor of 3 [53]. Observations like these do suggest a significant influence of particulate impurities on observable nucleation rates and thus need to be considered when interpreting homogeneous nucleation rate data.

For the alternative mechanism of homogeneous nucleation from dense reversible solute aggregates, a solid/liquid interface can influence the nucleation process only under two conditions: (i) when the surface intersects with the volume of a reversibly formed dense region that has the propensity to form a stable nucleus and (ii) when it also presents a nucleation site that allows a significantly faster assembly of a stable nucleus than in the dense solution region. To assess condition (i), we need to determine the rate by which large aggregates are formed within a solution volume, V_{het}, adjacent to a particle surface. If

this rate exceeds the homogeneous nucleation rate, then heterogeneous nucleation may be possible, if condition (ii) is also fulfilled.

For assessing condition (i), we must consider the solution volume with a thickness equal to the radius of a reversibly aggregated region around the particle. Outside this zone, reversible aggregates will not be intersected by the particle surface. Assuming the particle has a spherical shape with a diameter d, the situation sketched in Figure 1 applies. The volume of the potential heterogeneous nucleation zone is given by the thickness δ of the relevant interfacial solution region as

$$V_{het} = \frac{4}{3}\pi\left(\frac{d+\delta}{2}\right)^3 - \frac{4}{3}\pi\left(\frac{d}{2}\right)^3 = \frac{1}{6}\pi\left[(d+\delta)^3 - d^3\right]. \quad (16)$$

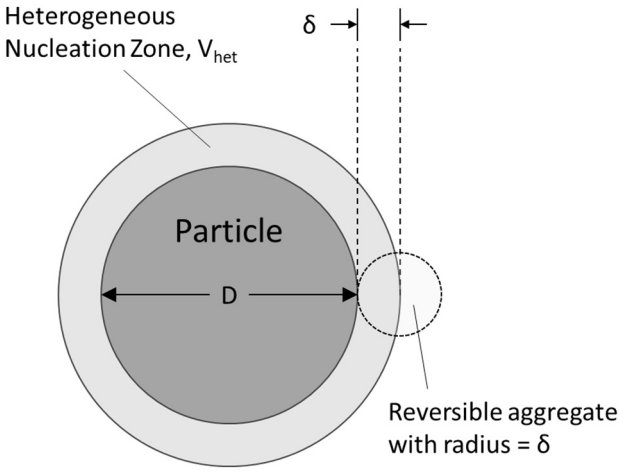

Figure 1. Geometric model for estimating the likelihood of heterogeneous nucleation on particles of solid impurities.

The rate by which the steady state population N^* of excess reversible aggregates contributing to the homogenous nucleation rate in a solution of volume V is formed is determined by the average aggregate lifetime, τ

$$\frac{dN^*}{dt} \approx \frac{N^*}{\tau}. \quad (17)$$

If all excess aggregates formed within V_{het} nucleate heterogeneously, the heterogeneous nucleation rate, in terms of the number of particles in the solution N_{part}, would be

$$J^*_{het} \approx \frac{N^*}{V\tau}\frac{V_{het}}{V}N_{part}, \quad (18)$$

which we can combine with Equation (16) and the definition of the homogeneous nucleation rate in Equation (15) to obtain

$$\frac{J^*_{het}}{J^*} \approx \frac{1}{6}\pi\left[(d+\delta)^3 - d^3\right]\frac{N_{part}}{V\tau k^*}. \quad (19)$$

This equation predicts that heterogeneous nucleation becomes more likely when the number of particles, N_{part}, in the solution increases as the size, d, of the particles increases and the thickness, δ, of the relevant interfacial volume, V_{het}, becomes larger. Heterogeneous nucleation becomes less likely as the solution volume, V, increases (decreasing particle concentration), the longer the lifetime of the aggregates (lower rate of excess aggregate formation, hence less likelihood of intersecting with a surface), and the higher the rate constant, k^*, for homogeneous nucleation.

The aggregate lifetime, τ, can be estimated from the solute–solute collision frequency, Z_{AA}, which depends, for spherical objects, on the concentration, $[M]_0$, and the dynamic viscosity, η, of the solution via the Stoke–Einstein–Sutherland equation for the diffusion coefficient, D [54],

$$Z_{AA} \approx 8\pi r D [M]_0 N_A = 8\pi r \frac{k_B T}{6\pi\eta r} [M]_0 N_A = \frac{4k_B T}{3\eta} [M]_0 N_A, \quad (20)$$

where r is the radius of a solute molecule and T the temperature. The lifetime, τ, of reversible aggregates of size n^* shall be estimated as

$$\tau \approx \frac{n^*}{Z_{AA}}, \quad (21)$$

which assumes diffusive dissociation of an aggregate of size n^* will require n^* individual and sequential events redispersing solvated solute molecules into the bulk of the solution.

The thickness, δ, of the relevant interfacial solution volume can be estimated from the molar volumes $V_{m,sol}$ and $V_{m,solv}$ of the solute and solvent molecules, respectively (via the mass densities and molar masses of the pure solutes and solvents). Assuming that every solute molecule is solvated by two solvent molecules, the total volume, V_{agg}, of an aggregate of n^* solvated solute molecules is approximately

$$V_{agg} \approx \frac{n^*}{N_A} (V_{m,sol} + 2V_{m,solv}) \quad (22)$$

Assuming that these aggregates are spherical, the thickness, δ, is equal to their radius and can be calculated by

$$\delta \approx \left(\frac{V_{agg}}{4\pi} \right)^{\frac{1}{3}}. \quad (23)$$

It should be stressed that these estimates for δ and τ, and indeed the whole framework for examining the likelihood of heterogeneous nucleation, are not meant to establish a quantitative theory of heterogeneous nucleation. They are merely meant to enable the task of examining, qualitatively, the possible relevance of heterogeneous pathways in homogeneous crystal nucleation. A truly predictive, quantitative theory of heterogeneous crystal nucleation at solid/liquid interfaces is yet to be developed.

3. Results

3.1. Effect of Supersaturation on the Size Distribution of Reversible Aggregates

The predicted impact of the supersaturation ratio, S, on the reversible aggregate size distribution in a solution is illustrated in Figure 2 for the specific case of 1 cm^3 of a meta-aminobenzoic acid (m-ABA) solution in an ethanol/water mixture at 25 °C. The solubility $[M]_0$ for this system was reported to be 0.128 mol dm^{-3} [21]. The calculated supersaturation-dependent reversible aggregate size concentrations in this plot have been normalized to their value at $S = 2.25$ because absolute concentrations vary by approximately 20 orders of magnitude as a function of aggregate size. The concentrations of monomers and small aggregates scale near-linearly with the supersaturation ratio. In contrast, the concentrations of the largest aggregates, with sizes of approximately $n \geq n^*$, exhibit a near-exponential rise with supersaturation that has striking similarity with the functional form of supersaturation-dependent nucleation rates. This is consistent with the central hypothesis of the model, namely, that homogeneous crystal nucleation from solution takes place predominantly from the largest reversible aggregates in a supersaturated solution. Indeed, this idea aligns with the well-established notion that in a saturated solution with the solubility concentration $[M]_0$, the rates of crystal nucleation and dissolution are equal and associated predominantly with the largest aggregates [10,33].

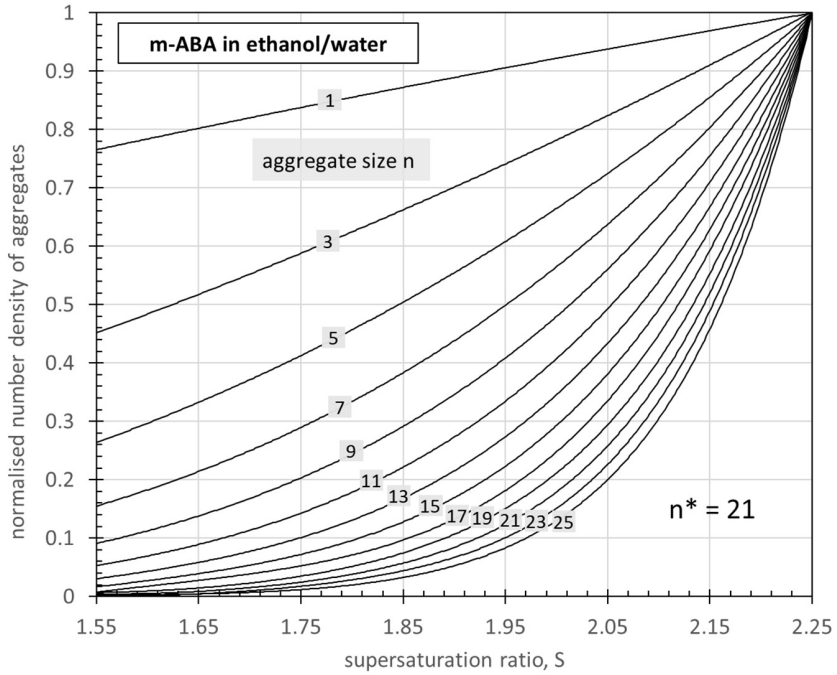

Figure 2. Predicted supersaturation-dependent size distribution of reversible aggregates in solutions of meta-aminobenzoic acid (m-ABA) in 1 cm^3 of an ethanol/water mixture at 25 °C. All aggregate concentrations are normalized to their value at S = 2.25. The size of the largest reversible aggregate in saturated solution is n* = 21.

3.2. Excess of Large Reversible Aggregates

To illustrate the concept of nucleation from the largest excess reversible aggregates further, the supersaturation-dependent size distribution of the largest aggregates of m-ABA is shown in Figure 3. The near-exponential increase in the reversible m-ABA aggregate count with sizes $n \geq n^*$ in 1 cm^3 solution is evident (note the logarithmic scale of the y-axis). At the solubility concentration (S = 1), the solution contains a single aggregate with n = 21, in line with the predicted n^* = 21 from Equation (12), and no aggregates with n > 21. The effect of increasing supersaturation is a near-exponential rise in the population of aggregates with larger sizes. For example, at S = 2.4, the aggregate size distribution extends to n = 29.

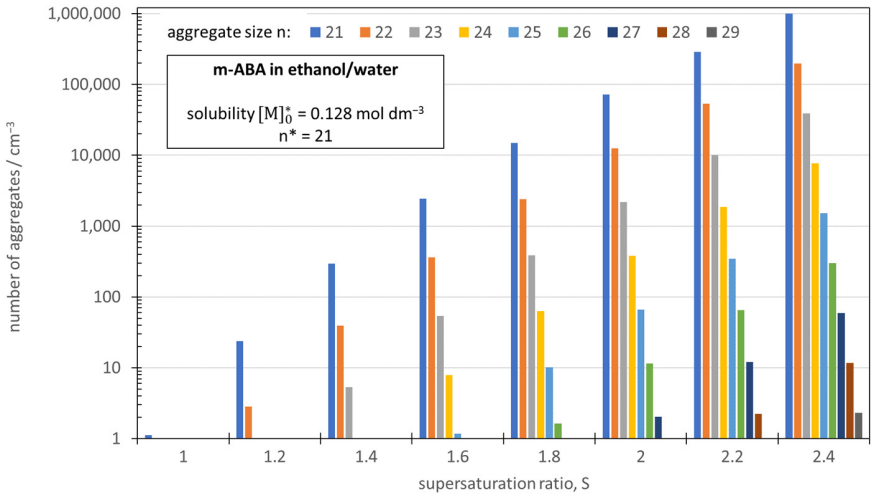

Figure 3. Supersaturation-dependent size distribution of reversible aggregates with sizes n equal to or higher than the largest aggregate size n^* = 21 in 1 cm^3 of a saturated solution of m-ABA in 50wt% ethanol in water.

3.3. Rate Constant Determination for m-ABA Crystallization from 50wt% Ethanol/Water

The fitting analysis of the rate predicted by Equation (15) against experimental J data for the m-ABA/ethanol/water system [21] is illustrated in Figure 4. Least-squares fitting of Equation (15) to the experimental data by variation of the rate constant k^* results in a best fit value for k^* of 8.2×10^{-9} s^{-1}. The curve reproduces the experimental data well. On first sight, the deviation to the nucleation rate at the highest supersaturation may seem substantial relative to the much better fit at lower supersaturations. However, the fit deviates by a maximum of ~5% from all experimental supersaturation values, well within the systematic and statistical errors that are expected to arise the experimental determination of nucleation rates [55]. In the next section, the same analysis will be applied to 10 other systems, with similar agreement between experiment and theory. The results will show that increased deviations at high supersaturation are not an intrinsic shortcoming of the model. Moreover, even with the expected substantial error margins on experimental data [55], meaningful results for k^* can be obtained because a fit of a single parameter function against a set of noisy datapoints produces a parameter value with a lower error margin, provided that the noise is predominantly random in nature.

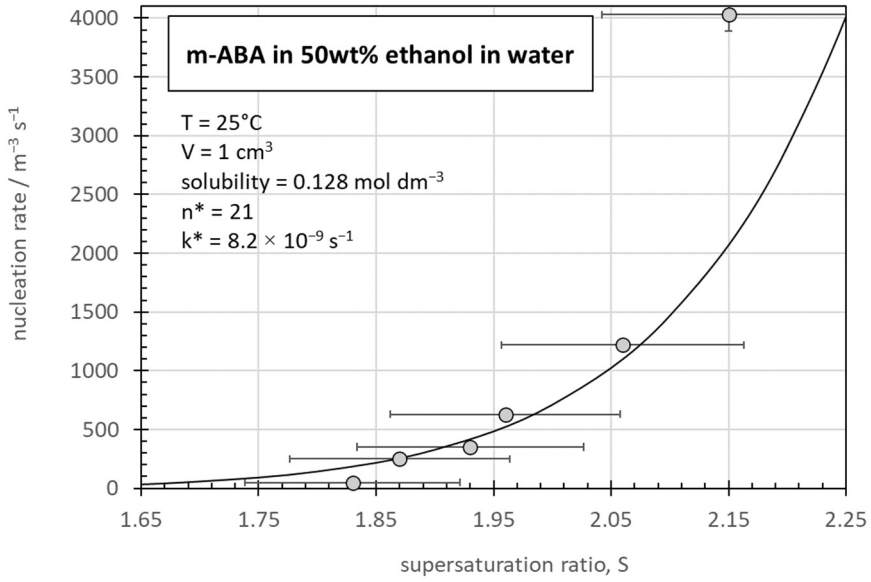

Figure 4. Predicted nucleation rate, J^*, (line) calculated from the reported solubility [21] with Equation (15) vs. experimental J data for m-ABA crystallization from 1 cm^3 ethanol/water (50wt%) [21]. Error bars for the nucleation rate [21] have been included. Error bars for S were not reported in [21], but experimental errors are likely on the order of ±5% or more for S. See ref. [55] for a deeper discussion of statistical errors associated with the small volume nucleation rate determinations employed for the measurements. The values for n^* and k^* indicated in the figure are the size of the largest reversible aggregates in the saturated solution (S = 1) and of the nucleation rate constant k^* obtained through the best fit procedure.

3.4. Nucleation Rates of 10 Benzoic Acid and para-Substituted Benzoic Acid Systems

To demonstrate the universal nature of the alternative approach, and to examine its relevance for relating solute–solute interactions to nucleation rates and the associated kinetic selection of polymorphic forms [56–58], previously published data for 10 binary solute–solvent systems, all containing benzoic acid or para-substituted benzoic acids as solutes [56,58,59], have been analyzed. The systems span combinations of four different solutes (benzoic acid, BA; para-aminobenzoic acid, pABA; para-nitrobenzoic acid, pNBA; para-toluic acid, pTA) with five solvents (water; ethyl acetate, EA; acetonitrile, MeCN; isopropanol, IPA; toluene, Tol), with solubilities varying by more than an order of magnitude from approximately ~0.03 to ~0.57 mol dm^{-3}.

As for aqueous m-ABA in ethanol/water, the fitting analyses achieve very good agreement with experimental nucleation rates for all systems (Figure 5, Table 1), indicating a general applicability of the proposed model. The pTA and BA solutions in toluene are likely to contain carboxylic acid dimers [60,61], so the analysis for these systems was performed assuming the presence of dimers.

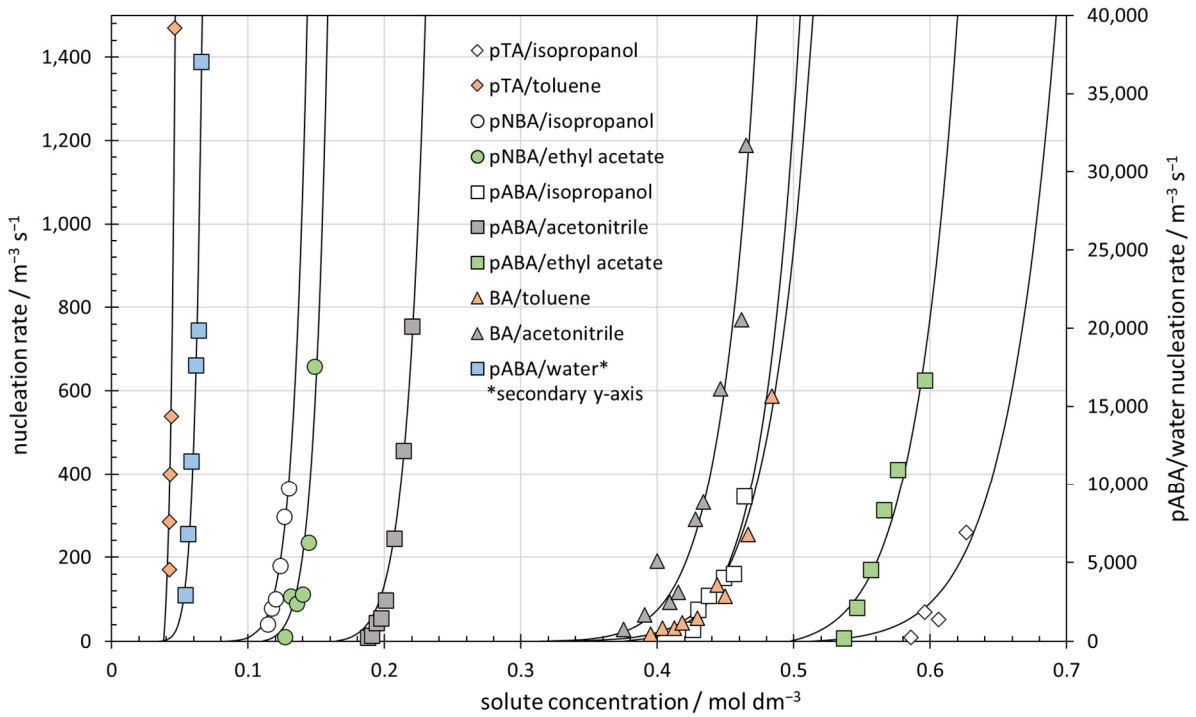

Figure 5. Predicted nucleation rates (full lines), J^*, calculated from reported solubilities [56,58,59] with Equation (15) vs. experimental data for para-toluic acid (pTA) in isopropanol and toluene [58], for para-nitrobenzoic acid (pNBA) in ethyl acetate and isopropanol [58], for para-aminobenzoic acid (pABA) in ethyl acetate, acetonitrile, and isopropanol [58], for pABA in water [56,59], and for benzoic acid (BA) in acetonitrile and toluene [58]. The solubilities, rate constants, k^*, and minimum rate-contributing aggregate sizes, n^*, are given in Table 1. The fits are reported as a function of the absolute solute concentration (rather than the supersaturation ratio, S), because this permits presentation of all data as a single figure; a set of corresponding plots as a function of the supersaturation ratio is provided in the Supporting Information, SI4. Reference [55] provides a discussion of statistical errors associated with the small volume nucleation rate determinations by which the nucleation rate data were measured.

The reproduction of the varying functional forms of the experimental nucleation rate curves with the single parameter model is remarkable: the steep increase in the nucleation rates for systems with low solubility is as well reproduced as the more gently increasing rates in the high solubility systems. The supersaturation dependence of nucleation rates is clearly well captured, as can also be seen in the same fits plotted as a function of the supersaturation ratio (Supporting Information, SI4). No system exhibits strong deviations between experimental data and model fits. Apart from the rate constant, k^*, the functional form of the calculated rate curves is predicted well by the concentration- (and hence supersaturation-) dependent reversible aggregate size distribution. The determined nucleation rate constants, k^*, span a range from ~10^{-8} s^{-1} for benzoic acid in toluene and p-nitrobenzoic acid in isopropanol to over 10^{-5} s^{-1} for p-toluic acid in toluene.

Table 1. Summary of solubilities, $[M]_0$, the supersaturation ratio S_{200} required to obtain a nucleation rate of 200 m^{-3} s^{-1}, the determined first order rate constants, k^*, the largest reversible aggregate sizes in saturated solution, n^*, for the stated temperatures for para-toluic acid (pTA) in isopropanol and toluene [58], for para-nitrobenzoic acid (pNBA) in ethyl acetate and isopropanol [58], for para-aminobenzoic acid (pABA) in ethyl acetate, acetonitrile, and isopropanol [58], for pABA in water [56,59], and for benzoic acid (BA) in acetonitrile and toluene [58]. The solubilities were determined as described in the cited papers alongside the nucleation rates.

Solute	Solvent	$[M]_0$/mol dm^{-3}	T/°C	S_{200}	k*/s^{-1}	n*
p-toluic acid	isopropanol	0.509	20	1.23	1.1×10^{-6}	36
	toluene #	0.038 #	20	1.08	4.1×10^{-5} #	14 #
p-nitrobenzoic acid	isopropanol	0.078	25	1.60	2.8×10^{-8}	17
	ethyl acetate	0.109	25	1.28	4.1×10^{-6}	20
p-aminobenzoic acid	isopropanol	0.374	20	1.22	3.1×10^{-6}	32
	acetonitrile	0.163	20	1.26	3.4×10^{-6}	23
	ethyl acetate	0.497	20	1.13	9.2×10^{-6}	36
	water	0.032	20	1.35	6.4×10^{-7}	13
benzoic acid	toluene #	0.286 #	20	1.59	1.2×10^{-8} #	28 #
	acetonitrile	0.310	20	1.37	1.8×10^{-7}	29

the solute species is assumed to be a carboxylic acid dimer

It has previously been pointed out that experimental nucleation rates of pABA in water appear to be high relative to those in organic solvents [56,59,62]. Within the framework of nucleation from reversible aggregates, the aqueous system does not stand out: the rate constant, k^*, of 6.4×10^{-7} s^{-1} is, in fact, somewhat lower than the rate constants determined for pABA in the other three solvents (Table 1). In line with this, nucleation from water requires a somewhat higher supersaturation ratio, S_{200}, of 1.35 (vs. 1.13, 1.22 and 1.26) to achieve a nucleation rate of 200 m^{-3} s^{-1} (Table 1), but the values of both k^* and S_{200} remain comparable to those for pABA nucleation from the organic solvents. The high nucleation rates for water are merely associated with the range of supersaturation ratios, S, chosen for the experimental rate measurements [56,59,62], which exceed S_{200} by far.

3.5. Homogeneous vs. Heterogeneous Nucleation

The strong variations in k^* suggest that the nucleation pathways, and thus the nature of the transition states for nucleation, vary significantly from system to system. Prima facie this would suggest that heterogeneous nucleation events are not as dominant as an analysis in the framework of CNT [49] may predict. The experimental determinations of nucleation rate data used in this paper appear to have been performed using unfiltered solvents and solutions, while the crystalline solute materials were not purified with a view to removing solid impurities. To assess whether heterogeneous nucleation 'seeded' by solid impurities was likely, Equation (19) was used to estimate its influence. The analysis by Equation (19) was performed assuming the presence of 320 spherical particles with a diameter of 0.1 µm in a volume of 1 mL, which are recently reported values for deionized tap water [48]. The results for J^*_{het}/J^* (Table 2) do suggest that heterogeneous nucleation would not be overwhelmingly dominant for this level of solid impurity contamination. The systems most likely to be affected are pNBA/isopropanol, BA/toluene, and mABA/50wt%ethanol/water, which are the three systems with the lowest nucleation rate constants, k^* (Table 1). It must be kept in mind as well that the calculated values represent a worst-case scenario. This point that will be taken up again in the discussion section below.

Table 2. Assessment of the likely relevance of heterogeneous nucleation through Equation (19). The analysis assumed V = 1 mL solution with N_{part} = 320 spherical particles with a diameter *d* of 0.1 µm.

Solute	Solvent	$V_{m,sol}$ cm^3	$V_{m,solv}$ cm^3	V_{agg} 10^{-27} m^3	δ nm	η mPa s	τ ns	$\frac{J^*_{het}}{J^*}$
p-toluic acid	isopropanol	128.4	76.5	16.8	1.1	0.237	5	1.0
	toluene	128.4	106.9	10.9	1.0	0.560	62	0.0
p-nitro-benzoic acid	isopropanol	105.8	76.5	7.3	0.8	0.237	16	9.7
	ethyl acetate	105.8	97.7	10.0	0.9	0.455	25	0.0
p-amino-benzoic acid	isopropanol	99.8	76.5	13.4	1.0	0.237	6	0.3
	acetonitrile	99.8	52.2	7.8	0.9	0.334	14	0.1
	ethyl acetate	99.8	97.7	17.6	1.1	0.455	10	0.1
	water	99.8	18.0	2.9	0.6	0.890	109	0.0
benzoic acid	toluene	96.5	106.9	18.9	1.1	0.560	16	29.5
	acetonitrile	96.5	52.2	9.7	0.9	0.334	9	2.7
m-ABA	50wt% ethanol/water	90.8	18.0	4.4	0.7	0.890	44	9.9

4. Discussion

4.1. Homogeneous vs. Heterogeneous Nucleation

Because the experimental values for the nucleation rate constant, *k**, vary by several orders of magnitude, they influence the predictions made by Equation (19) more than the other relevant parameters given in Table 2. In interpreting the results of these estimates for the significance of heterogeneous nucleation, it needs to be kept in mind that Equation (19) was derived assuming that *any* intersection of a surface with a reversible aggregate large enough to facilitate homogeneous nucleation will lead to a heterogeneous nucleation event. From a transition state theory point of view, it appears unlikely that any contact with a solid surface will inevitably trigger a nucleation event because the formation of the transition state for a stable crystal nucleus will still require some specific spatiotemporal organization of solute and solvent molecules. This, as the nucleation rate constants, *k**, attest, occurs very rarely even in the largest reversible aggregates in a solution. Heterogeneous nucleation by the route proposed in Section 2.3 would therefore likely be governed by rate constants of similar magnitudes, reflecting similar transition states, unless, of course, a completely different nucleation route is taken, e.g., templating of a different nucleus structure.

For unfiltered solutions with a higher level of solid impurities than the 320 particles assumed in the model calculation, heterogeneous nucleation may indeed take place with an appreciable or even dominant rate, but the determined *k** values would likely reflect the formation of transition states similar or even identical to those through the homogeneous route. The reported small reduction in the nucleation rate for isonicotinamide crystallization from ethanol after removing particles with sizes > 0.45 µm [53] appears to be consistent with this proposition. It has also been reported that nano-sized (diameters ~1 nm) impurities are likely present in solutions with extremely high number densities [63], but these impurities would likewise not remove the need for assembling the complex transition state. They may perhaps appear as inclusions in nuclei formed in their neighborhood (note also that 1 nm is of a similar size as the reversible aggregate sizes).

This is not to say that heterogeneous nucleation via reversible aggregates is impossible. By adding sufficiently high levels of solid particulate material, a technique commonly used in seeded crystallization and templating of different crystal habits and polymorphic forms [52], one can increase the likelihood of heterogeneous nucleation so that it becomes inevitable. According to Equation (19), just adding 100 particles with a diameter of 100 µm per ml of solution would increase the likelihood of heterogeneous nucleation by approximately five orders of magnitude.

The analysis of nucleation rates in the framework of homogeneous nucleation via reversible aggregates thus appears to be less sensitive than CNT to the presence of heteroge-

neous nucleation centers, because the structure of the nucleus is determined synergistically by a collection of molecules in a transition state that should not differ radically between homogeneous and heterogeneous routes. Rates of homogeneous nucleation and heterogeneous nucleation on microscopic impurities may therefore be more similar than an analysis in the framework of CNT would suggest. The observed strong variations in k^* between different systems, the reproducibility of nucleation rate measurements in different laboratories, with different solvent batches and different suppliers of solute materials, by and large appear to be consistent with this conclusion as well.

4.2. Interpretation of the Constants n and k**

Across all systems examined, the reversible aggregate size, n^*, in saturated solution varies from 13 for aqueous pABA to 36 for pTA/isopropanol and pABA/ethyl acetate (Table 1). The universal non-linear correlation between solubility and the value of n^* is evident from the plot of these values in Figure 6a. The line superimposed over the data represents Equation (12). Some datapoints slightly deviate from this curve because of the rounding of aggregate sizes to the nearest integer. This solubility dependence of the minimum size of nucleating aggregates may just be a consequence of the relationship between the thermodynamic stabilities of a solute in the solid and the solution phases: solubility is lower when the solid phase of the pure solute is more stable. Higher cohesive energies can be expected to stabilize critical crystal nuclei as well, which may therefore nucleate from smaller reversible aggregates.

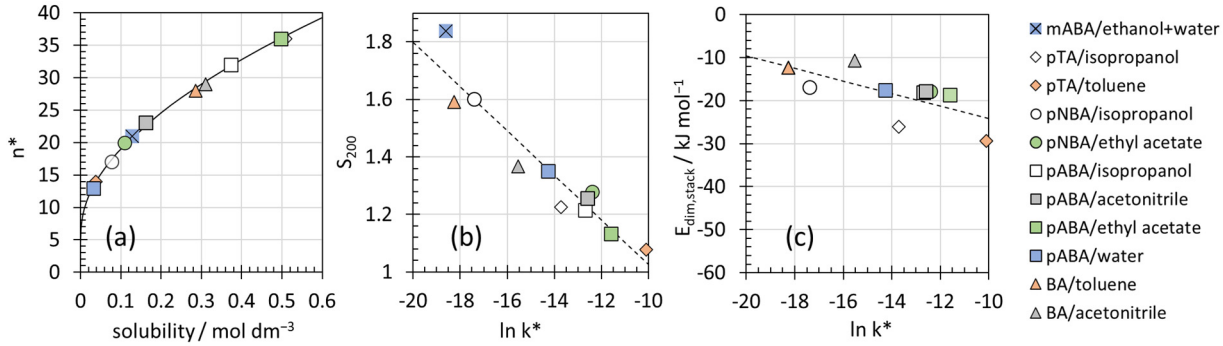

Figure 6. (**a**) Predicted dependence of the largest aggregate size, n^*, in saturated solutions of the solute/solvent systems listed on the right. (**b**) Supersaturation ratios required for a nucleation rate of 200 m^{-3} s^{-1} (S_{200}) as a function of ln(k^*). (**c**) Correlation between calculated energies of aromatic dimer stacking interactions [58] and ln(k^*).

In contrast to n^*, the values for the nucleation rate constant, k^*, are system-specific, and no significant correlation with the solubility is evident from the values reported in Table 1. However, k^* is the dominant factor determining absolute nucleation rates. This is demonstrated easily by examining its relationship with the supersaturation ratio required to achieve a fixed nucleation rate. The supersaturation required for an arbitrarily chosen nucleation rate of 200 m^{-3} s^{-1}, S_{200}, has previously [58] been used to compare the systems included in Figure 6. The original motivating idea for choosing a benchmark rate is that its value should increase with the height of the nucleation barrier. Using the influence of the supersaturation ratio on N^*, Equation (15), we can now evaluate the relationship between S_{200} and k^*. S_{200} decreases almost exponentially as a function of k^*, resulting in a near-linear dependence of S_{200} on $\ln(k^*)$ that is only weakly dependent on the overall solution concentration, $[M]_0$ (Supplementary Information, SI3). Not surprisingly, therefore, across all benzoic acid systems examined, there is also a significant correlation between S_{200} and $\ln(k^*)$, as shown in Figure 6b. This correlation can be readily understood by invoking the expected Arrhenius behavior of the rate constant, k^*, which is associated with an activation energy, E_A, and a pre-exponential factor, A, according to

$$\ln(k^*) = \ln(A) - \frac{E_A}{RT}. \quad (24)$$

For a given temperature, S_{200} is therefore expected to correlate with ln(A) and/or the activation energy, E_A. Without temperature-dependent rate measurements, which are not available for these systems, it is not possible to separate the effects of A and E_A. However, it is interesting to note that a strong correlation between S_{200} and the energy associated with aromatic dimer stacking interactions in solution ($E_{dim,stack}$) was also reported [58]. These aromatic dimer interaction energies should predominantly manifest as variations in the attractive forces between reversibly aggregated solvated solute molecules, i.e., they probably influence E_A more than A. Within the framework of nucleation from reversible aggregates, the correlation between $E_{dim,stack}$ and S_{200} thus becomes a correlation with ln(k^*), as shown in Figure 6c. It was suggested [58] that the correlation with $E_{dim,stack}$ reflects varying degrees of pre-ordering through aromatic stacking interactions in the pre-nucleation state, which influences the rate of crystal nucleation, thereby achieving, inter alia, kinetic control of the crystal structure. The analysis in terms of nucleation driven by reversible aggregation provides a different angle to this hypothesis: the dimer stacking interactions may influence E_A and hence k^*, which would be a classical Arrhenius interpretation of the proposed kinetic control. Temperature-dependent studies should be able to shed more light on this.

4.3. Some General Points

Like CNT, the reversible aggregation model includes the notion of a critical minimum size of aggregates, as crystal nuclei appear to be formed predominantly from the largest reversible aggregates. A size dependence is expected to arise for two reasons: first, nuclei that can continue to grow to crystals must be sufficiently long-lived and resilient to re-dissolution. They may therefore have to exceed a critical size, and the required number of solute molecules may only be available in the largest reversible aggregates. Second, assembling the transition state to nucleation would require a complex spatiotemporal alignment of multiple solvated solute and solvent molecules. The likelihood that such an assembly occurs spontaneously increases with the volume of the dense regions. These and other mechanistic hypotheses, e.g., whether desolvation dynamics influence the nucleation rate, need to be explored further in the future by analyzing k^* variations for more systems, performing research into the ultrafast dynamics of nucleation processes, and by modelling of transition states with molecular dynamics and statistical mechanical analysis.

Finally, the most striking consequence of considering reversible aggregates as the loci of homogeneous nucleation events is that supersaturation merely drives a pre-equilibrium to nucleation, which determines the number density of nucleation centers. The rate constant, k^*, for nucleation, and hence the exponential barrier term that follows from the classic Arrhenius expression for the rate constant, are much less dependent on supersaturation. As has been pointed out before [32–34,64], the chemical kinetics approach provides a framework that integrates the influence of mass action (overall solute concentration), thermodynamics (properties of the overall solution, the dense regions formed by reversible aggregation, activation enthalpy and activation entropy of the transition state) with a molecular level view (structure and dynamics of solvated solute molecules, the transition state and the nucleus). The use of chemical kinetics thus has the advantage of considering nucleation more generally as a dynamic assembly process resulting from molecular interactions in the initial state of the system. It removes any prescription of final state thermodynamics, as for example the surface tension and bulk cohesion arguments used in CNT [65], which assumes that the rate determining step is associated with desolvated crystal nuclei, which would be an example for Hammond's notion of a late transition state [66]. The theoretical framework resulting from the chemical kinetics approach thus goes a long way towards a vision [7,22] of integrating the thermodynamics and macroscopic kinetics of homogeneous

nucleation with an atomistic view amenable to molecular modelling, statistical mechanical analysis, and advanced experimental studies of molecular and electronic structure.

5. Conclusions

The hypothesis of homogeneous nucleation from dense solution regions formed by reversible aggregation has been found to lead to a mathematical expression that predicts the supersaturation dependence of homogeneous organic crystal nucleation rates quantitatively from solubility with only one empirical parameter, a system-specific overall rate constant, k^*. This expression has tremendous practical value because a single accurate nucleation rate measurement at one supersaturation is in principle sufficient to determine k^*, allowing the prediction of the supersaturation dependence of the homogeneous nucleation rate at the temperature of the measurement. A central feature of this alternative mechanistic framework for modelling homogeneous nucleation from solution is that the rate constant can be linked to an activated complex with a specific molecular structure in the transition state, providing the missing framework [22] for integrating molecular dynamics with nucleation rate measurement and advanced experimental characterization of the structure of nuclei and nucleating solutions. This integrates homogeneous nucleation theory with the extensive body of absolute rate theory analysis methods developed in the chemical sciences over the last century [1–4]. At the molecular level, the concept of homogeneous nucleation in regions of high solute density seems to be akin to macromolecular folding, e.g., of proteins [67], which is also associated with spatiotemporally demanding breaking and forming of multiple bonds, including solvent release. The challenge for future research is to develop an understanding of the value of k^* through establishing the sequence(s) of elementary steps that lead to the formation of the transition state. The dynamics and structure of the transition state are not only expected to determine the nucleation rate, but likely also influence the selection of the crystal structure in the final product.

Supplementary Materials: The following supporting information can be downloaded at: https://www.mdpi.com/article/10.3390/cryst14040349/s1, Full derivations of Equations (10) and (12) and the relationship between S_{200} and $\ln(k^*)$, alternative plots of the data in Figure 5 as a function of supersaturation.

Funding: This research was financially supported by EPSRC through the Future Continuous Manufacturing and Advanced Crystallisation (CMAC) Hub (EP/P006965/1) as well as by the Royal Academy of Engineering, Diamond Light Source and Infineum UK Ltd., through the RAEng Bragg Centenary Chair.

Data Availability Statement: All data supporting this study are provided either in the results section of this paper or in the electronic Supplementary Information accompanying it.

Acknowledgments: I would like to thank Philip J Camp for pointing out that the reversible aggregation mass balance can be calculated through a geometric/power series, obsoleting my original brute-force approach through coupled differential equations. I am grateful to Elizabeth A Willneff for sharing the dissatisfaction with the status quo and encouragement to publish, and to Joop ter Horst for comments on the early development of my thinking. I would like to thank the reviewers of this paper who gave unusually thorough feedback that has improved the manuscript very significantly.

Conflicts of Interest: The author declares no conflict of interest.

References

1. Glasstone, S.; Laidler, K.J.; Eyring, H. *The Theory of Rate Processes*, 1st ed.; McGraw-Hill, Inc.: New York, NY, USA; London, UK, 1941.
2. Atkins, P.W. *Physical Chemistry*, 6th ed.; Oxford University Press: Oxford, UK, 1998.
3. Laidler, K.J. *Chemical Kinetics*; Harper & Row: New York, NY, USA, 1987.
4. Bao, J.L.; Truhlar, D.G. Variational Transition State Theory: Theoretical Framework and Recent Developments. *Chem. Soc. Rev.* **2017**, *46*, 7548–7596. [CrossRef] [PubMed]
5. Laidler, K.J. Symbolism and Terminology in Chemical Kinetics. *Pure Appl. Chem.* **1981**, *53*, 753–771. [CrossRef]
6. Kashchiev, D.; Van Rosmalen, G.M. Review: Nucleation in Solutions Revisited. *Cryst. Res. Technol.* **2003**, *38*, 555–574. [CrossRef]

7. Davey, R.J.; Schroeder, S.L.M.; Ter Horst, J.H. Nucleation of Organic Crystals—A Molecular Perspective. *Angew. Chemie-Int. Ed.* **2013**, *52*, 2166–2179. [CrossRef] [PubMed]
8. Yi, P.; Rutledge, G.C. Molecular Origins of Homogeneous Crystal Nucleation. *Annu. Rev. Chem. Biomol. Eng.* **2012**, *3*, 157–182. [CrossRef] [PubMed]
9. Sosso, G.C.; Chen, J.; Cox, S.J.; Fitzner, M.; Pedevilla, P.; Zen, A.; Michaelides, A. Crystal Nucleation in Liquids: Open Questions and Future Challenges in Molecular Dynamics Simulations. *Chem. Rev.* **2016**, *116*, 7078–7116. [CrossRef]
10. Kashchiev, D. *Nucleation: Basic Theory with Applications*; Butterworth-Heinemann: Oxford, UK, 2000.
11. Myerson, A.S.; Erdemir, D.; Lee, A.Y. Crystal Nucleation. In *Handbook of Industrial Crystallization*; Cambridge University Press: Cambridge, UK, 2019; pp. 76–114. ISBN 9781139026949.
12. Li, X.; Wang, J.; Wang, T.; Wang, N.; Zong, S.; Huang, X.; Hao, H. Molecular Mechanism of Crystal Nucleation from Solution. *Sci. China Chem.* **2021**, *64*, 1460–1481. [CrossRef]
13. Mullin, J.W. *Crystallization*, 4th ed.; Butterworth-Heinemann: Oxford, UK, 2001.
14. Volmer, M.; Weber, A. Keimbildung in Übersättigten Gebilden. *Zeitschrift Fur Phys. Chemie* **1926**, *119*, 277–301. [CrossRef]
15. Becker, R.; Döring, W. Kinetische Behandlung Der Keimbildung in Übersättigten Dämpfen. *Ann. Phys.* **1935**, *24*, 719–752. [CrossRef]
16. Volmer, M. *Kinetik Der Phasenbildung*; Steinkopff: Leipzig, Germany, 1939.
17. Wu, D.T.; Gránásy, L.; Spaepen, F. Nucleation and the Solid-Liquid Interfacial Free Energy. *MRS Bull.* **2004**, *29*, 945–950. [CrossRef]
18. Oxtoby, D.W. Homogeneous Nucleation—Theory and Experiment. *J. Physics-Condensed Matter* **1992**, *4*, 7627–7650. [CrossRef]
19. Turnbull, D.; Fisher, J.C. Rate of Nucleation in Condensed Systems. *J. Chem. Phys.* **1949**, *17*, 71–73. [CrossRef]
20. Black, S. Simulating Nucleation of Molecular Solids. *Proc. R. Soc. A-Math. Phys. Eng. Sci.* **2007**, *463*, 2799–2811. [CrossRef]
21. Jiang, S.; Ter Horst, J.H. Crystal Nucleation Rates from Probability Distributions of Induction Times. *Cryst. Growth Des.* **2011**, *11*, 256–261. [CrossRef]
22. Blow, K.E.; Quigley, D.; Sosso, G.C. The Seven Deadly Sins: When Computing Crystal Nucleation Rates, the Devil Is in the Details. *J. Chem. Phys.* **2021**, *155*, 40901. [CrossRef]
23. Guo, H.; Liu, K. Control of Chemical Reactivity by Transition-State and Beyond. *Chem. Sci.* **2016**, *7*, 3992–4003. [CrossRef] [PubMed]
24. Polanyi, J.C.; Zewail, A.H. Direct Observation of the Transition State. *Acc. Chem. Res.* **1995**, *28*, 119–132. [CrossRef]
25. Einstein, A. Über Die von Der Molekularkinetischen Theorie Der Wärme Geforderte Bewegung von in Ruhenden Flüssigkeiten Suspendierten Teilchen. *Ann. Phys.* **1905**, *322*, 549–560. [CrossRef]
26. von Smoluchowski, M. Zur Kinetischen Theorie Der Brownschen Molekularbewegung Und Der Suspensionen. *Ann. Phys.* **1906**, *326*, 756–780. [CrossRef]
27. Chandrasekhar, S. Stochastic Problems in Physics and Astronomy. *Rev. Mod. Phys.* **1943**, *15*, 1–89. [CrossRef]
28. Bentz, J.; Nir, S. Mass Action Kinetics and Equilibria of Reversible Aggregation. *J. Chem. Soc. Faraday Trans. 1 Phys. Chem. Condens. Phases* **1981**, *77*, 1249–1275. [CrossRef]
29. Jeffrey, G.C.; Ottewill, R.H. Reversible Aggregation Part 2. Kinetics of Reversible Aggregation. *Colloid Polym. Sci.* **1990**, *268*, 179–189. [CrossRef]
30. Vasilev, G.A.; Filkova, A.A.; Sveshnikova, A.N. Study of Reversible Platelet Aggregation Model by Nonlinear Dynamics. *Mathematics* **2021**, *9*, 759. [CrossRef]
31. Girshick, S.L.; Chiu, C.P. Kinetic Nucleation Theory: A New Expression for the Rate of Homogeneous Nucleation from an Ideal Supersaturated Vapor. *J. Chem. Phys.* **1990**, *93*, 1273–1277. [CrossRef]
32. Katz, J.L.; Wiedersich, H. Nucleation Theory without Maxwell Demons. *J. Colloid Interface Sci.* **1977**, *61*, 351–355. [CrossRef]
33. Katz, J.L.; Spaepen, F. A Kinetic Approach to Nucleation in Condensed Systems. *Philos. Mag. B Phys. Condens. Matter; Stat. Mech. Electron. Opt. Magn. Prop.* **1978**, *37*, 137–148. [CrossRef]
34. Chiang, P.P.; Donohue, M.D.; Katz, J.L. A Kinetic Approach to Crystallization from Ionic Solution. II. Crystal Nucleation. *J. Colloid Interface Sci.* **1988**, *122*, 251–265. [CrossRef]
35. Vekilov, P.G. Two-Step Mechanism for the Nucleation of Crystals from Solution. *J. Cryst. Growth* **2005**, *275*, 65–76. [CrossRef]
36. Gebauer, D.; Kellermeier, M.; Gale, J.D.; Bergström, L.; Cölfen, H. Pre-Nucleation Clusters as Solute Precursors in Crystallisation. *Chem. Soc. Rev.* **2014**, *43*, 2348–2371. [CrossRef]
37. Kashchiev, D.; Vekilov, P.G.; Kolomeisky, A.B. Kinetics of Two-Step Nucleation of Crystals. *J. Chem. Phys.* **2005**, *122*, 244706. [CrossRef]
38. Vekilov, P.G. The Two-Step Mechanism of Nucleation of Crystals in Solution. *Nanoscale* **2010**, *2*, 2346–2357. [CrossRef] [PubMed]
39. Erdemir, D.; Lee, A.Y.; Myerson, A.S. Nucleation of Crystals from Solution: Classical and Two-Step Models. *Acc. Chem. Res.* **2009**, *42*, 621–629. [CrossRef] [PubMed]
40. Kashchiev, D. Classical Nucleation Theory Approach to Two-Step Nucleation of Crystals. *J. Cryst. Growth* **2020**, *530*, 125300. [CrossRef]
41. Karthika, S.; Radhakrishnan, T.K.; Kalaichelvi, P. A Review of Classical and Nonclassical Nucleation Theories. *Cryst. Growth Des.* **2016**, *16*, 6663–6681. [CrossRef]
42. De Yoreo, J. A Perspective on Multistep Pathways of Nucleation. *ACS Symp. Ser.* **2020**, *1358*, 1–17. [CrossRef]

43. Li, J.; Deepak, F.L. In Situ Kinetic Observations on Crystal Nucleation and Growth. *Chem. Rev.* **2022**, *122*, 16911–16982. [CrossRef] [PubMed]
44. Jun, Y.S.; Zhu, Y.; Wang, Y.; Ghim, D.; Wu, X.; Kim, D.; Jung, H. Classical and Nonclassical Nucleation and Growth Mechanisms for Nanoparticle Formation. *Annu. Rev. Phys. Chem.* **2022**, *73*, 453–477. [CrossRef]
45. Yang, F.; Yuan, K.; Stack, A.G.; Starchenko, V. Numerical Study of Mineral Nucleation and Growth on a Substrate. *ACS Earth Space Chem.* **2022**, *6*, 1655–1665. [CrossRef]
46. Gebauer, D.; Gale, J.D.; Cölfen, H. Crystal Nucleation and Growth of Inorganic Ionic Materials from Aqueous Solution: Selected Recent Developments, and Implications. *Small* **2022**, *18*, 2107735. [CrossRef]
47. Smoluchowski, M.V. Versuch Einer Mathematischen Theorie Der Koagulationskinetik Kolloider Lösungen. *Zeitschrift Für Phys. Chemie* **1918**, *92U*, 129–168. [CrossRef]
48. Popov, K.; Oshchepkov, M.; Kovalenko, A.; Redchuk, A.; Dikareva, J.; Pochitalkina, I. Scale Nucleation Natural Precursors: A Case Study of "Micro/Nanodust" Impurities Nature in Laboratory Aqueous Samples Obtained from Moscow Tap Water. *Int. J. Corros. Scale Inhib.* **2020**, *9*, 1097–1112. [CrossRef]
49. Liu, X.Y. Heterogeneous Nucleation or Homogeneous Nucleation? *J. Chem. Phys.* **2000**, *112*, 9949–9955. [CrossRef]
50. Rausch, H.; Sziklai, I.L.; Nazarov, V.M.; Bodon, P.; Erdélyvári, I.; Tóth, B. Determination of Impurities in High-Purity Solvents by Neutron Activation Analysis. *J. Radioanal. Nucl. Chem.* **1991**, *148*, 217–225. [CrossRef]
51. Gebauer, D. How Can Additives Control the Early Stages of Mineralisation? *Minerals* **2018**, *8*, 179. [CrossRef]
52. Nicoud, L.H.; Myerson, A.S. The Influence of Impurities and Additives on Crystallization. In *Handbook of Industrial Crystallization*; Cambridge University Press: Cambridge, UK, 2019; pp. 115–135. ISBN 9781139026949.
53. Kulkarni, S.A.; Kadam, S.S.; Meekes, H.; Stankiewicz, A.I.; Ter Horst, J.H. Crystal Nucleation Kinetics from Induction Times and Metastable Zone Widths. *Cryst. Growth Des.* **2013**, *13*, 2435–2440. [CrossRef]
54. Debye, P. Reaction Rates in Ionic Solutions. *Trans. Electrochem. Soc.* **1942**, *82*, 265–272. [CrossRef]
55. Xiao, Y.; Tang, S.K.; Hao, H.; Davey, R.J.; Vetter, T. Quantifying the Inherent Uncertainty Associated with Nucleation Rates Estimated from Induction Time Data Measured in Small Volumes. *Cryst. Growth Des.* **2017**, *17*, 2852–2863. [CrossRef]
56. Black, J.F.B.; Cardew, P.T.; Cruz-Cabeza, A.J.; Davey, R.J.; Gilks, S.E.; Sullivan, R.A. Crystal Nucleation and Growth in a Polymorphic System: Ostwald's Rule,: P -Aminobenzoic Acid and Nucleation Transition States. *CrystEngComm* **2018**, *20*, 768–776. [CrossRef]
57. Tang, S.K.; Davey, R.J.; Sacchi, P.; Cruz-Cabeza, A.J. Can Molecular Flexibility Control Crystallization? The Case of Para Substituted Benzoic Acids. *Chem. Sci.* **2021**, *12*, 993–1000. [CrossRef]
58. Cruz-Cabeza, A.J.; Davey, R.J.; Sachithananthan, S.S.; Smith, R.; Tang, S.K.; Vetter, T.; Xiao, Y. Aromatic Stacking—A Key Step in Nucleation. *Chem. Commun.* **2017**, *53*, 7905–7908. [CrossRef]
59. Sullivan, R.A. Molecules, Clusters, Crystals: The Crystallisation of p-Aminobenzoic Acid from Solution. Ph.D. Thesis, The University of Manchester, Manchester, UK, 2015.
60. Sullivan, R.A.; Davey, R.J.; Sadiq, G.; Dent, G.; Back, K.R.; Ter Horst, J.H.; Toroz, D.; Hammond, R.B. Revealing the Roles of Desolvation and Molecular Self-Assembly in Crystal Nucleation from Solution: Benzoic and p -Aminobenzoic Acids. *Cryst. Growth Des.* **2014**, *14*, 2689–2696. [CrossRef]
61. Hanrahan, E.S.; Bruce, B.D. Dimerization of P-Substituted Benzoic Acids. *Spectrochim. Acta Part A Mol. Spectrosc.* **1967**, *23*, 2497–2503. [CrossRef]
62. Turner, T.D.; Corzo, D.M.C.; Toroz, D.; Curtis, A.; Dos Santos, M.M.; Hammond, R.B.; Lai, X.; Roberts, K.J. The Influence of Solution Environment on the Nucleation Kinetics and Crystallisability of Para-Aminobenzoic Acid. *Phys. Chem. Chem. Phys.* **2016**, *18*, 27507–27520. [CrossRef] [PubMed]
63. Trukhina, M.; Tkachenko, S.; Ryabova, A.; Oshchepkov, M.; Redchuk, A.; Popov, K. Calcium Sulfate Crystallization in Presence of Fluorecent-Tagged Polyacrylate and Some Refinement of Scale Inhibition Mechanism. *Minerals* **2023**, *13*, 559. [CrossRef]
64. Katz, J.L.; Donohue, M.D. A Kinetic Approach to Homogeneous Nucleation Theory. In *Advances in Chemical Physics*; Prigogine, I., Rice, S.A., Eds.; John Wiley & Sons, Inc.: New York, NY, USA; Chichester, UK; Brisbane, Australia; Toronto, ON, Canada, 1979; Volume 40, pp. 137–156.
65. Ruckenstein, E.; Djikaev, Y.S. Recent Developments in the Kinetic Theory of Nucleation. *Adv. Colloid Interface Sci.* **2005**, *118*, 51–72. [CrossRef] [PubMed]
66. Hammond, G.S. A Correlation of Reaction Rates. *J. Am. Chem. Soc.* **1955**, *77*, 334–338. [CrossRef]
67. Eaton, W.A. Modern Kinetics and Mechanism of Protein Folding: A Retrospective. *J. Phys. Chem. B* **2021**, *125*, 3452–3467. [CrossRef]